12th IFAC International Symposium on
Advanced Control of Chemical Processes
July 14-17, 2024. Toronto, Canada

# Towards Pilot-Scale Electric Arc Furnace Temperature Prediction & Bath Size Estimation with Long Short-Term Memory Networks

**Antony Gareau-Lajoie** * **Daniel Rodrigues** **
**Marie-Ève Gosselin** ** **Moncef Chioua** *

* *Department of Chemical Engineering, Polytechnique Montréal, Montréal, QC, Canada (e-mail: antony.gareau-lajoie@polymtl.ca)*
** *Critical Minerals and Technology Centre, Rio Tinto Iron and Titanium Quebec Operations, Sorel-Tracy, QC, Canada*

**Abstract:** A safe and reliable operation of electric arc furnaces (EAFs) is crucial for the mining and mineral industries. The lack of continuous measurements of critical process variables, such as the bath size of the molten phase, makes this operation challenging. Additionally, operator support decision tools able to predict the evolution of key process variables such as furnace sidewall temperatures would help to maintain safe operations. The present work proposes a data-driven (DD) modeling procedure to develop (1) a predictive model of the sidewall temperature and, (2) an online bath size estimator. Both sidewall temperature predictor and bath size estimator are based on long short-term memory (LSTM) networks. The preliminary developed models are validated on datasets collected on an industrial pilot-scale EAF and show good performance.

*Keywords:* Data-driven Modeling, Electric Arc Furnace, Machine Learning Assisted Modeling, Process metallurgy

## 1. INTRODUCTION

Process plants in operation in the mining and mineral industries are complex and large-scale systems that require advanced distributed control systems for their control, their monitoring and for supporting operator's decision-making. One limiting factor of such systems is the lack of continuous measurements of key process variables. These key variables are essential for the safety of the operation and the quality control of final and intermediate products (Ke et al., 2017).

Electric Arc Furnaces (EAFs) are pyrometallurgical process units used to upgrade ore to a desired metallic content. To reach fusion, ore and reagents fed to the unit are heated via an electric arc generated by two electrodes located on the top side of the EAF. (Zietsman, 2004). A liquid phase called *molten bath* is progressively generated from ore heated to high temperatures. A major danger is a leak of molten material through the equipment. This event is called a *run-out* and can happen when the sidewall temperatures are too high or when the refractory layer thickness is reduced due to wearing (Joubert and Kotze, 2019). On the other hand, maximizing the EAF production capacity requires maximizing the bath size, leading to unsafe operation. This is why reliable tracking of bath size is important for operations.

Monitoring of the furnace sidewall temperature profile uses several thermocouples. This temperature profile is key to a safe operation. Molten content stays solid on the inner perimeter of refractory bricks. This solid phase is called *freeze lining*. It allows slowing down the wear of the refractory lining (Joubert and Kotze, 2019). Monitoring the refractory wall thickness of the EAF is challenging as it cannot be directly measured (Leon-Medina et al., 2022). Instead, the bath size is used as a proxy of the wall thickness and is estimated using the mass of liquid metal collected at each tapping phase and electrodes positions before and after each tapping phase.

Significant efforts are made to develop first principle (FP) models with computational fluid dynamics (CFD) methods explaining hydrodynamics, heat transfers and interactions between phases occurring in the unit (Odenthal et al., 2018). To take into account the actual operating conditions and chemistry of the bath, FP models need to be calibrated to process measurements (Rodrigues et al., 2023). While improving the model accuracy, FP model calibration does not solve another limitation of FP that prevents them from being deployed online: their high computation time (Hosain and Fdhila, 2015).

Data-driven (DD) models are well suited for online deployment. In recent years, machine learning (ML) models have been proposed to develop data-driven models used as soft-sensors in chemical and metallurgical processes. Such ML models include multi-layer perceptron (MLP) (Souza et al., 2019) and recurrent neural networks (RNN) such as long short-term memory (LSTM) (Ke et al., 2017). LSTM networks solve the vanishing gradient issue found in standard RRNs (Noh, 2021) and do lend themselves to the

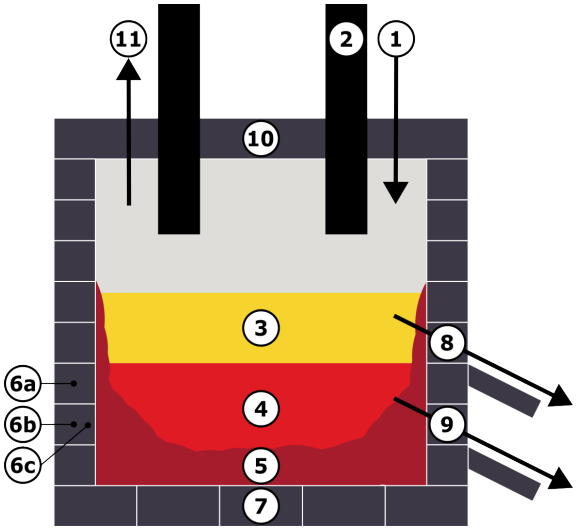


Fig. 1. Electric arc furnace main elements locations. (1) Ore and reagent inlet; (2) Electrodes; (3, 4) Molten bath products 1 and 2; (5) Freeze lining; (6a, 6b, 6c) Thermocouples at various heights and depths; (7) Refractory bricks; (8, 9) Tap-holes for products 1 and 2; (10) Water-cooled roof; (11) Gas outlet.

modeling of non-linear dynamic systems. An arrangement of layers of LSTM cells, activation functions and fully connected layers architecture called *stacked* LSTM is used in (Kim et al., 2019) to predict remaining time to close tap-holes in a blast furnace. Stacked LSTM architecture will be used for bath size estimation.

Electric arc furnaces temperature prediction using long short-term memory (LSTM) networks are presented in (Godoy-Rojas et al., 2022), while multi-target regression is used in (Leon-Medina et al., 2022).

To the author's best knowledge, no data-driven model for the online estimation of bath size in EAF processes has been proposed in the literature.

In this work, we propose an alternative approach for the prediction of electric arc furnaces temperature based on feature engineering. Dimension reduction with principal component analysis (PCA) is a feature engineering method that has been used for product quality prediction of metallurgical processes (Xin et al., 2023). Other methods use phenomenological process knowledge to engineer features (Hongyang Li et al., 2022). Both of these methods will be used in the feature engineering step of the proposed approach.

The contributions of this paper are twofold :

(1) Development of an EAF sidewall temperature predictor using a sequence-to-sequence LSTM network with engineered input features.
(2) Development of an EAF bath size estimator using a sequence-to-one LSTM network with engineered features and measured inputs.

The remaining of the paper is organized as follows: Section 2 provides a short overview of the EAF process and its operation. Section 3 details the proposed approach to develop a sidewall temperature predictor and a bath size estimator. Both LSTM-based networks general methodology will also be detailed. Section 4 describes an application of the proposed methodology on a pilot-scale EAF three-day test campaign dataset. Section 5 concludes the paper with some weakness of the approach and suggests future steps for improvement.

## 2. ELECTRIC ARC FURNACES OPERATION DESCRIPTION

EAF are operated in a semibatch mode. The furnace is continually filled with ore and reagent. Once the furnace is full, it is emptied through a *tap-hole* during the tapping phase, after which, the tap-hole is sealed. The bath size at the end of the taping phase is estimated using the ratio between the mass of recovered molten material and the bath level variation. These two values are manually measured at the end of the taping phase by an operator. High bath size values indicate a low freeze lining thickness, which can result in refractory wear (Zietsman, 2004). While direct molten bath temperature measurements of EAFs can be done using costly disposable probes (Blažič et al., 2021), sidewall temperatures measurements are usually preferred for continuous monitoring because thermocouples, being further away from the molten bath, are exposed to lower temperatures. Thermocouples used for temperature measurements are inserted in the furnace sidewall at multiple heights and depths. Sidewall temperatures reflect the molten bath temperature but are affected by the size and the thermal conductivity of both sidewall and freeze lining (Joubert and Kotze, 2019).

## 3. PROPOSED APPROACH

A model predicting the EAF sidewall temperature over a sliding time horizon is proposed. This sequence-to-sequence model takes as input engineered features described in Section 3.1. A second model, estimating the bath size between tapping phases, is also proposed. This is a sequence-to-one model that takes as inputs process measurements in addition to engineered features described in Section 3.2.

### *3.1 Feature Engineering for Temperature Prediction*

Instead of the EAF sidewall temperature $T_{Sidewall}$, the temperature increment $\Delta T_{Sidewall}$ representing the difference between two consecutive temperature measurements is used as input to the sidewall temperature predictor. This local linearization approach that considers a small range of temperature values over the predicted horizon, improved convergence and performance of the model.

### *3.2 Feature Engineering for Bath Size Estimation*

Bath size estimator uses simple features calculated from the measured electric power consumed by the EAF and estimated ore and reagent mass flows. These features are accumulated values of electric power ($P^{Integrated}$) and mass flows ($Q_{Ore}^{Integrated}$, $Q_{Reagent}^{Integrated}$) between tapping phase periods. Accumulated values are set to zero after each tapping phase. Training bath size estimator using

accumulated values instead of raw measurements of electric power and mass flows helped the model capturing the integrator dynamics of the system. Algorithm 1 presents the pseudocode of the implemented method.

**Algorithm 1** Numerical Integration With Reset

**Input:** Process measurements vector, Reset index (tapping phases)
**1.** Initialize an empty integrated feature vector
**2.** Initialize a cumulative variable for integrated values
**3. for** each value of process measurements vector **do**
  **4.** Compute a numerical integration on the current and past value in process measurements vector
  **5.** Update the cumulative variable
  **6.** Append the cumulative variable to the current integrated feature vector
  **if** Current reset index is equal to the process measurement index **do**
    Set cumulative variable = 0
    Set current reset index to its next value
  **else** pass
**Output:** Integrated feature

Implementation of Algorithm 1 is made using *SciPy* Python library (Virtanen et al., 2020). Note that the size of the integrated feature vector is one less than the original vector because of the chosen numerical integration method.

Principal component analysis (PCA) based dimensional reduction is applied to temperature measurements collected from the cooling and the sidewall monitoring systems. Resulting features denoted $PCA(T_{cw}, T_{Sidewall})$ were three principal components used to retain 90 % of the total dataset variability. The pseudocode steps presented in Algorithm 2 describe the implemented method.

**Algorithm 2** Dimension Reduction With PCA

**Input:** Measurements matrix, Explained variance limit
**1.** Compute the directions of maximal variance in vector-valued data by performing PCA on the model inputs matrix
**while** Total explained variance $\leq$ Explained variance limit **do**
  **2.** Compute the current principal component explained variance.
  **3.** Add current explained variance to total explained variance.
**4.** Extract dimensionally reduced features matrix
**Output:** Dimensionally reduced features matrix

Implementation of Algorithm 2 is made using Scikit-learn Python module (Pedregosa et al., 2011).

### *3.3 Network Architectures*

A simplified version of a stacked LSTM architecture (Kim et al., 2019) has been selected for the bath size model, and a single LSTM is used for the temperature model. The number of hidden nodes and layers need to be determined empirically in accordance with the complexity of the predicting task. Hyperparameters such as the learning rate, the optimization algorithm, and the number of epochs also had to be determined for both models, to reach acceptable performances in terms of error metric defined in Section 3.4. A weight dropout probability is adjusted for regularization purposes to prevent co-adaptation (Hinton et al., 2012). It avoids local minima convergence. Both models are implemented and tested using *PyTorch* library (Paszke et al., 2019).

### *3.4 Error Metric*

Mean absolute percentage error (MAPE) is well adapted to sequence-to-one bath size estimation. MAPE considers the prediction error for each time step. Equation 1 details the MAPE error metric. Differences between the process measurement value $y_i$ at time step $i$ and its predicted value $\hat{y}_i$ are averaged over the $N$ samples of the dataset.

$$\text{MAPE}(y, \hat{y}) = \frac{100\%}{N} \sum_{i=1}^{N} \left| \frac{y_i - \hat{y}_i}{y_i} \right| \tag{1}$$

Averaged absolute percentage error (AMAPE) is well adapted to sequence-to-sequence temperature prediction model performance evaluation. AMAPE groups the error of each predicted sequence at every time step into a single performance value. Error metrics can be averaged over forecasting horizon of multi-step forecasting applications (Sangiorgio and Dercole, 2020). Equation 2 details the computation of AMAPE error metric. Differences between the process measurement value $y_i$ at time step $i$ and its predicted value, $\hat{y}_i$ are averaged over the predicted horizon $H$. The errors of all predicted sequences are then averaged over the $N$ samples of the dataset.

$$\text{AMAPE}(y, \hat{y}) = \frac{1}{N} \sum_{i=1}^{N} \frac{100\%}{H} \sum_{i=1}^{H} \left| \frac{y_i - \hat{y}_i}{y_i} \right| \tag{2}$$

### *3.5 Data Preparation and Model Training Procedure*

Computed features and raw process measurements are first merged. Next, the merged dataset is segmented to several windows of past measurement samples and features. For the model inputs, each window is of size $L$, a predefined hyperparameter adjusting the *lookback period*. For the model outputs (labels), each window is of size $H$, the prediction horizon length. Figure 2 summarizes the steps of the dataset transformation.

Next, data is normalized using standardization as defined in Equation 3 where $\mu$ is the mean and $\sigma$ the standard deviation computed over the time dimension.

$$y_i^{Scaled} = \frac{y_i - \mu}{\sigma} \tag{3}$$

The dataset is split in subsets (70%-15%-15%). A calibration set used to train the ML model, a validation set used for hyperparameter tuning, and a test set used to evaluate the model performance. Using a grid search, parameters and hyperparameters are iteratively adjusted to ensure convergence and to achieve an acceptable level of performance. The list of parameters and hyperparameters that were modified for both models is:

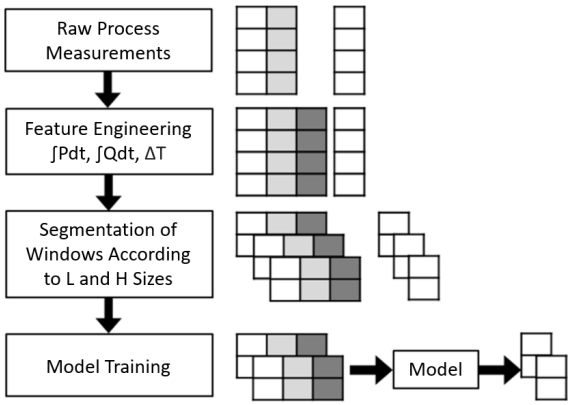


Fig. 2. Dataset transformation to include features in windows used in model training

- Features and measurements selected as input
- Size of lookback sequences ($L$)
- Size of prediction horizon ($H$) [Sidewall temperature]
- Network architecture (single or stacked LSTM)
- Number of hidden nodes in LSTM cells
- Number of layers in LSTM cells
- Number of epochs
- Dropout probability
- Learning rate

The learning rate and the weight dropout probability are manually set. Adam algorithm was used for optimization.

## 4. INDUSTRIAL CASE STUDY

Process measurements from a pilot-scale EAF operated by Rio Tinto Iron and Titanium Quebec Operations were collected during a three-day test campaign and used to validate the proposed approach. A predicted horizon of 90 minutes was deemed to be adequate for the operators monitoring the EAF sidewall temperature and for process operation adjustments. Process operators also expressed an interest in having access to an online bath size estimation between consecutive tapping phases to ensure a safe EAF operation.

The present section describes the collected EAF dataset followed by a performance evaluation of a sidewall temperature prediction model and of a bath size estimation model, both developed using the collected dataset. Results of a single sidewall temperature prediction model are presented. To predict the profile over space of sidewall temperatures, the same methodology can be repeated for different sidewall temperatures but is out of the scope of the present work. Note that all process variable values are normalized for the purpose of confidentiality.

### *4.1 Dataset Description*

The dataset used in this work includes nine types of process variables measured on the pilot-scale EAF and listed in Table 1. Multiple sidewall temperatures and cooling water temperatures are recorded at various heights and depths using thermocouples. Estimated mass flows of ore and reagents are available. Bath size is the result of manual measurements performed at each tapping phase.

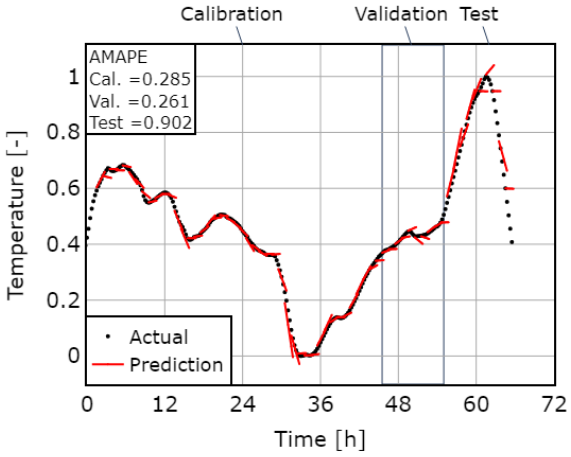


Fig. 3. Sidewall temperature prediction from feature input $\Delta T_{Sidewall}$ (best model in validation performances)

### *4.2 Preprocessing*

The raw dataset is extracted from the plant process historian, where compressed high frequency measurements are stored. Raw process data are down sampled, using a standard average pooling, to a constant sampling period of 15 minutes. Data are then standardized and split in three sets as described in Section 3.5.

### *4.3 Sidewall Temperature Prediction Results Analysis*

Figure 3 displays, in black, all the resampled points of a single thermocouple located in the EAF sidewall. The best model predictions are visible, in red, but only one in every six prediction sequence is shown for clarity (1/6). Every sequence was used to calculate the error metric AMAPE displayed in the upper-left corner. Three AMAPE values are shown corresponding to the calibration, validation and test datasets.

Among the different process measurements and features used in the training of the sidewall temperature predictor, the best input was a single feature ($\Delta T_{Sidewall}$). A grid search of range of 60, 90 and 120 minutes for the lookback value $L$, of range 1 or 2 LSTM cells layers and of range 64, 128 and 256 for the number of hidden nodes was conducted. The grid search led to an $L$ optimal value of 90 minutes, a number of layers of 1 and a number of hidden nodes of 128 for a single LSTM architecture.

Table 1. EAF process variables used for models development

| Signal name | Symbol | Unit |
|---|---|---|
| Sidewall temperatures | $T_{Sidewall}$ | $°C$ |
| Cooling water temperatures | $T_{cw}$ | $°C$ |
| Power input | $P$ | $kW$ |
| Ore Power Ratio | $OPR$ | $kg/kWh$ |
| Ore Reagent Ratio | $ORR$ | $kg/kg$ |
| Ore mass flow | $Q_{Ore}$ | $kg/h$ |
| Reagent mass flow | $Q_{Reagents}$ | $kg/h$ |
| Electrode position | $EL$ | $cm$ |
| Bath size | $B$ | $kg/cm$ |

A relative good fit of the calibration dataset was to be expected given the low dynamics of the temperature but, greater performances in validation than in calibration was not. A possible explanation would be that the system was less disturbed in the narrow validation time window. Closer to stationary conditions sequences might be easier to predict. The last dataset was the test set and the model shown lesser performances trying to predict it.

Table 2 shows the AMAPE values obtained using the selected hyperparameters values. For the test dataset, the AMAPE value is 0.90 %. Thermocouple temperature had been directly used as input and achieved an AMAPE of 4.02 %, in the best case, for the same test dataset.

Table 2. Sidewall temperature prediction improvement using $\Delta_T$ as input

| | AMAPE (%) | | |
|---|---|---|---|
| Input | Calibration | Validation | Test |
| $T_{Sidewall}$ | 2.68 | 2.44 | 4.02 |
| $\Delta T_{Sidewall}$ | 0.28 | 0.26 | 0.90 |

Some observations in the test set were greater in value than what was previously seen in the training. Moreover, a steep descent was only seen at relatively lower temperatures, which would explain the higher error for the test dataset.

The generally high accuracy obtained can be explained by the fact that the actual temperature variability within the predicted sequence of 90 minutes is relatively low. Slow dynamic response of the process temperature to a change in operation makes temperature measurements that are close in time highly correlated. This important inertia is visible in Figure 3.

### *4.4 Bath Size Estimation Results Analysis*

Figure 4 shows measured bath size at the end of every tapping phase in black. At the resampling frequency is displayed the estimation of the bath size between tapping phases in red. The error metric of the calibration, validation and test dataset is shown in the upper-left corner. Note that error evaluation is only possible at tapping phases.

Bath size estimator inputs that allowed the best performances were a combination of process measurements and manually extracted features ($P$, $OPR$, $ORR$, $P^{Integrated}$, $Q_{Ore}^{Integrated}$, $Q_{Reagent}^{Integrated}$, $PCA(T_{CW}, T_{Sidewall})$). A grid search was performed over a range of 60, 90 and 120 minutes for the lookback value $L$, 1 or 2 LSTM cells layers and a range of 32, 64, 128 and 256 for the number of hidden nodes. The grid search led to an optimal value of $L$ of 90 minutes, a number of layers of 1 and a number of hidden nodes of 32 for a stacked LSTM architecture.

In validation and test set, some bath size measurements were well modeled. However, it should be noted that high values of bath size could not be well modeled for the given dataset and training. Only one relatively high value is present in the calibration set, visible at around 16 h in Figure 4. More data could help cover a wider spectrum of the system response in the calibration set.

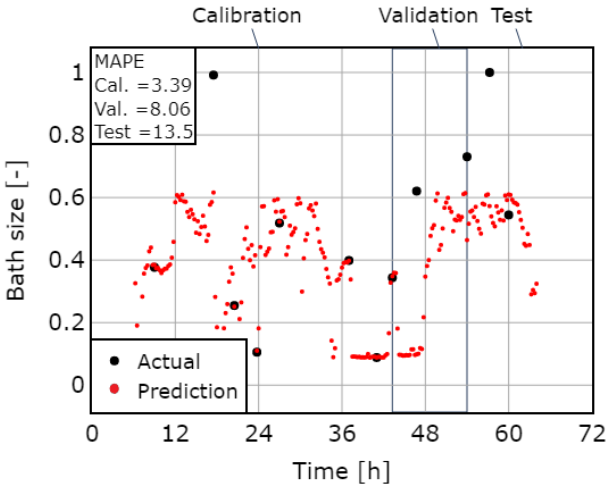


Fig. 4. Bath size estimation from raw measurements and features (best model)

## 5. CONCLUSION

Based on a three-day test campaign dataset of a pilot-scale EAF operations, two preliminary models were developed. First, a sequence-to-sequence predictor of 90 minutes of sidewall temperature was trained using 90 minutes lookback sequences of the feature ($\Delta T_{Sidewall}$). The lowest value found for sidewall temperature AMAPE is 0.90 % for the test dataset. Secondly, a sequence-to-one estimator was developed using a combination of features and process measurements ($P$, $OPR$, $ORR$, $P^{Integrated}$, $Q_{Ore}^{Integrated}$, $Q_{Reagent}^{Integrated}$, $PCA(T_{cw}, T_{Sidewall})$) to estimate the current bath size value, between tapping phases based on 90 minutes of lookback sequences. The lowest value found for the test dataset was a MAPE of 13.5 %. For both models, the use of features based on process knowledge and dimension reduction methods were pivotal to reach these performances.

Future work will be done with a larger dataset that will be available shortly. Additional data might help to mitigate some noted flaws of the current best models. Methods known to deal with small datasets like cross-validation, virtual sample generation (VSG) (Li et al., 2021), data augmentation (Heidrich et al., 2022) and transfer learning techniques (López Santos et al., 2023) will be evaluated in addition to the new dataset to improve performances.

## ACKNOWLEDGEMENTS

This work is supported equally from Rio Tinto Iron and Titanium Quebec Operations and from the Mitacs Accelerate program.

## REFERENCES

Blažič, A., Škrjanc, I., and Logar, V. (2021). Soft sensor of bath temperature in an electric arc furnace based on a data-driven takagi–sugeno fuzzy model. *Applied Soft Computing*, 113, 107949. doi: https://doi.org/10.1016/j.asoc.2021.107949.

Godoy-Rojas, D.F., Leon-Medina, J.X., Rueda, B., Vargas, W., Romero, J., Pedraza, C., Pozo, F., and Tibaduiza, D.A. (2022). Attention-based deep recurrent neural network to forecast the temperature behavior of an electric arc furnace side-wall. *Sensors*, 22(4), 1418. doi:10.3390/s22041418.

Heidrich, B., Mannsperger, L., Turowski, M., Phipps, K., Schäfer, B., Mikut, R., and Hagenmeyer, V. (2022). Boost short-term load forecasts with synthetic data from transferred latent space information. *Energy Informatics*, 5(1), 20. doi:10.1186/s42162-022-00214-7.

Hinton, G.E., Srivastava, N., Krizhevsky, A., Sutskever, I., and Salakhutdinov, R.R. (2012). Improving neural networks by preventing co-adaptation of feature detectors.

Hongyang Li, X.L., Liu, X., Bu, X., Li, H., and Lyu, Q. (2022). Prediction of blast furnace parameters using feature engineering and stacking algorithm. *Ironmaking & Steelmaking*, 49(3), 283–296. doi: 10.1080/03019233.2021.1992816.

Hosain, M.L. and Fdhila, R.B. (2015). Literature Review of Accelerated CFD Simulation Methods towards Online Application. *Energy Procedia*, 75, 3307–3314. doi: 10.1016/j.egypro.2015.07.714.

Joubert, H. and Kotze, H. (2019). Design of sidewall lining/cooling systems for ac or dc ilmenite smelting furnaces. In *unpublished*.

Ke, W., Huang, D., Yang, F., and Jiang, Y. (2017). Soft sensor development and applications based on lstm in deep neural networks. *2017 IEEE Symposium Series on Computational Intelligence (SSCI)*, 1–6. doi: 10.1109/SSCI.2017.8280954.

Kim, K., Seo, B., Rhee, S.H., Lee, S., and Woo, S.S. (2019). Deep Learning for Blast Furnaces: Skip-Dense Layers Deep Learning Model to Predict the Remaining Time to Close Tap-holes for Blast Furnaces. In *Proceedings of the 28th ACM International Conference on Information and Knowledge Management*, 2733–2741. ACM, Beijing China. doi:10.1145/3357384.3357803.

Leon-Medina, J.X., Camacho-Olarte, J., Rueda, B., Vargas, W., Bonilla, L., Ruiz, J., Sofrony, J., Guerra-Gomez, J.A., Restrepo-Calle, F., and Tibaduiza, D.A. (2022). Monitoring of the refractory lining in a shielded electric arc furnace: An online multitarget regression trees approach. *Structural Control and Health Monitoring*, 29(3), e2885. doi:https://doi.org/10.1002/stc.2885.

Li, L., Damarla, S.K., Wang, Y., and Huang, B. (2021). A Gaussian mixture model based virtual sample generation approach for small datasets in industrial processes. *Information Sciences*, 581, 262–277. doi: https://doi.org/10.1016/j.ins.2021.09.014.

López Santos, M., Díaz García, S., García-Santiago, X., Ogando-Martínez, A., Echevarría Camarero, F., Blázquez Gil, G., and Carrasco Ortega, P. (2023). Deep learning and transfer learning techniques applied to short-term load forecasting of data-poor buildings in local energy communities. *Energy and Buildings*, 292, 113164. doi:10.1016/j.enbuild.2023.113164.

Noh, S.H. (2021). Analysis of gradient vanishing of rnns and performance comparison. *Information*, 12(11). doi: 10.3390/info12110442.

Odenthal, H.J., Kemminger, A., Krause, F., Sankowski, L., Uebber, N., and Vogl, N. (2018). Review on Modeling and Simulation of the Electric Arc Furnace (EAF). *steel research international*, 89(1), 1700098. doi: 10.1002/srin.201700098.

Paszke, A., Gross, S., Massa, F., Lerer, A., Bradbury, J., Chanan, G., Killeen, T., Lin, Z., Gimelshein, N., Antiga, L., Desmaison, A., Kopf, A., Yang, E., DeVito, Z., Raison, M., Tejani, A., Chilamkurthy, S., Steiner, B., Fang, L., Bai, J., and Chintala, S. (2019). Pytorch: An imperative style, high-performance deep learning library. In *Advances in Neural Information Processing Systems 32*, 8024–8035. Curran Associates, Inc.

Pedregosa, F., Varoquaux, G., Gramfort, A., Michel, V., Thirion, B., Grisel, O., Blondel, M., Prettenhofer, P., Weiss, R., Dubourg, V., Vanderplas, J., Passos, A., Cournapeau, D., Brucher, M., Perrot, M., and Duchesnay, E. (2011). Scikit-learn: Machine learning in Python. *Journal of Machine Learning Research*, 12, 2825–2830.

Rodrigues, C.M.G., Wu, M., Ishmurzin, A., Hackl, G., Voller, N., Ludwig, A., and Kharicha, A. (2023). Modeling Framework for the Simulation of an Electric Smelting Furnace Considering Freeze Lining Formation. *Metallurgical and Materials Transactions B*, 54(2), 880–894. doi:10.1007/s11663-023-02733-4.

Sangiorgio, M. and Dercole, F. (2020). Robustness of LSTM neural networks for multi-step forecasting of chaotic time series. *Chaos, Solitons & Fractals*, 139, 110045. doi:10.1016/j.chaos.2020.110045.

Souza, A.M.F.d., Soares, F.M., Castro, M.A.G.d., Nagem, N.F., Bitencourt, A.H.d.J., Affonso, C.d.M., and Oliveira, R.C.L.d. (2019). Soft sensors in the primary aluminum production process based on neural networks using clustering methods. *Sensors*, 19(23), 5255. doi: 10.3390/s19235255.

Virtanen, P., Gommers, R., Oliphant, T.E., Haberland, M., Reddy, T., Cournapeau, D., Burovski, E., Peterson, P., Weckesser, W., Bright, J., van der Walt, S.J., Brett, M., Wilson, J., Millman, K.J., Mayorov, N., Nelson, A.R.J., Jones, E., Kern, R., Larson, E., Carey, C.J., Polat, İ., Feng, Y., Moore, E.W., VanderPlas, J., Laxalde, D., Perktold, J., Cimrman, R., Henriksen, I., Quintero, E.A., Harris, C.R., Archibald, A.M., Ribeiro, A.H., Pedregosa, F., van Mulbregt, P., and SciPy 1.0 Contributors (2020). SciPy 1.0: Fundamental Algorithms for Scientific Computing in Python. *Nature Methods*, 17, 261–272. doi:10.1038/s41592-019-0686-2.

Xin, Z., Zhang, J., Jin, Y., Zheng, J., and Liu, Q. (2023). Predicting the alloying element yield in a ladle furnace using principal component analysis and deep neural network. *International Journal of Minerals, Metallurgy and Materials*, 30(2), 335–344. doi:10.1007/s12613-021-2409-9.

Zietsman, J.H. (2004). *Interactions between freeze lining and slag bath in ilmenite smelting*. Thesis, University of Pretoria. Accepted: 2013-09-07T15:11:30Z.